




Ion-beam lithography for fabrication of diffractive optical phase elements in silver-ion-exchanged glasses

Arashmid Nahal^{1,*} , Seyed Reza Hosseini^{1,2}, and Masoud Mahjour-Shafiei²

¹ Photonic Materials Research Laboratory, Department of Physics, College of Science, University of Tehran, 1439955961 Tehran, Iran

² Ion Beam Research Laboratory, Department of Physics, College of Science, University of Tehran, 1439955961 Tehran, Iran

Received: 5 June 2021

Accepted: 11 August 2021

Published online:
24 August 2021

© The Author(s), under exclusive licence to Springer Science+Business Media, LLC, part of Springer Nature 2021

ABSTRACT

In the present article, ion-beam lithography in ion-exchanged glasses is used as a method for the fabrication of miniaturized phase optical diffractive elements. It is established that, as a result of the interaction of a low-energy (~ 40 keV) He^+ ion beam with silver-ion-exchanged glasses, the index of refraction of interacted area increases. In the interacted areas of the samples, the formation of neutral silver nanoparticles leads to an increase in the index of refraction. This paves the way to employ such material to produce optical phase diffractive elements such as slits, gratings, or Fresnel's zone plates. It is found that a remarkable dispersion for the index of refraction ($n = n(\lambda)$) gives rise to the dependence of diffraction efficiency of produced elements to the wavelength of the probe beams. The produced elements are of good quality, optically effective, chemically stable, waterproof, and scratch resistant.

1 Introduction

There are many detailed studies, in which, methods of preparation and fundamental optical and spectroscopic properties of the ion-exchanged glasses are presented and discussed [1–7]. The simplicity of the preparation methods of ion-exchanged glasses, which results in production of effective photonic materials (containing metallic nanoparticles), and also their wide applications as passive or active photonic miniaturized devices like, waveguides, and elements [8], could be considered as motivations for the above-mentioned researches. The ion-exchanged glasses are still in center of attention for more

advanced investigations due to their application as planar waveguide [9] and their plasmonic behaviors [10, 11]. The mechanism of the Ion-exchange process has already been studied in detail [3, 9, 12]. Interaction of the ion-exchanged glass with an external electric field [13, 14] and its interaction with laser beams in different conditions [5, 6, 15, 16] have also been studied. Results of the aforementioned researches show that any induced changes in size, geometry, electrical charge, or interaction with neighboring nanoclusters or the matrix (where the silver nanoclusters are embedded) would have significant effects on the photonic properties of the ion-exchanged glasses. Outcomes of the aforesaid studies

Address correspondence to E-mail: nahal@ut.ac.ir

emphasize the importance of improving new methods to enhance the induced changes in the optical properties of the ion-exchanged glasses, especially changing the index of refraction, which is a crucial functional parameter in the photonic devices and elements. There are other glass preparation methods, as a photonic material, which lead to increase of index of refraction of the glasses [17, 18] by adding materials like BaCO_3 and Nb_2O_5 to the glass composition. As they have remarkable interaction with high-energy ion beams or photons, they could be investigated as other candidates for ion-beam lithography base material.

In this order, following our previous studies and experiences [5, 6, 12–14], to achieve accurate, durable, and permanent changes in the index of refraction ($n = n(\lambda)$) in this material, we studied the interaction of an ion beam of a light atom such as “ He^+ ” with the ion-exchanged glass [19]. In the mentioned study, we could show what happens after the interaction, and how the index of refraction could be changed and manipulated by this method. Actually, as a result of the interaction of the ion beam with the ion-exchanged glass (i.e., ion-beam bombardment), the ionic silver nanoparticles reduce to the neutral ones. It results in increasing the index of refraction ($n(\lambda)$) and simultaneous quenching of the photoluminescence radiation of the interacted area on the sample, excited by a probe light. In [19], we have shown that quenching of the photoluminescence is related to the reduction of Ag_N^+ clusters to the neutral ones (Ag_N). As the formation of neutral silver clusters increases, the dielectric constant of the glass substrate in the depth where ion exchange has happened increases, which in its turn increases the refractive index of the interacted ion-exchanged layer. From the results of the mentioned study [19], we found that we can make miniaturized or even integrated optical diffractive elements such as Fresnel’s zone, diffraction gratings, slits, double slits, and other optical diffractive elements by patterning the index of refraction in the ion-exchanged glass using the low-energy ion beam. This method is called *ion-beam lithography*. In addition, it was found out that this method can be used to induce stable, long-lasting, and perfect patterns of $n(\lambda)$.

There are many studies in which the authors have tried to make some diffractive optical elements in the ion-exchanged glasses. Some of them have tried to use a high-power laser beam to make micro-lenses [20, 21], or make gratings [22]. The others have made

gratings applying a direct external electric field on a metallic mask on the surface of an ion-exchanged glass [23]. As an electron beam can interact with the ion-exchanged glass and produce neutral silver nanocrystalline [24], some researchers have tried to use a direct electron beam to do some kind of lithography on the glasses, doped by Nickel, and compared it with direct use of He^+ beam on the surface of their samples [25].

In this article, which is actually the second part of our previous article [19], we present the results of the ion-beam lithography in silver-ion-exchanged glasses using low-energy He^+ ions ($E_{\text{IB}} \sim 40 \text{ keV}$). The optical properties of the fabricated miniaturized diffractive optical elements, which are obtained by patterning and engineering the index of refraction using the mentioned method are discussed. The produced elements are of good quality, optically effective, chemically stable, and scratch resistant. That is, after washing the produced elements with water or even diluted acid, its optical properties did not change. We also observed that temperature tolerance from room temperature to $100 \text{ }^\circ\text{C}$ does not affect the index of refraction or diffraction efficiency of the produced diffractive elements.

2 Experimental

2.1 Preparation method for making one-sided ion-exchanged glass

The samples are made by well-known ion-exchange method [3, 5, 9]. The type of the glass substrate should be soda lime. The dimensions of the glass were $22 \text{ mm} \times 22 \text{ mm} \times 0.8 \text{ mm}$. The chemical combination of the glass and its components’ weight ratio influence on the depth of diffusion and also concentration of metal ions into the substrate [12]. By XRF analysis, the combination of the used glass substrate obtained as follows: (weight%: wt%) 74.466 wt% SiO_2 , 13.577 wt% Na_2O , 4.349 wt% MgO , 1.178 wt% Al_2O_3 , 0.304 wt% SO_3 , 0.856 wt% K_2O , 5.126 wt% CaO , 0.106 wt% As , and 0.009 wt% Zr . Based on our experiences and background, we chose silver ions to be exchanged. The soda-lime glass has enough Na^+ ions suitable for the ion-exchange process. In common manner of ion-exchanged sample preparation method, one inserts the glass slide into a molten $\text{NaNO}_3/\text{AgNO}_3$ mixed salt. Such treatment provides

two-sided ion-exchanged sample, which is not appropriate for our purposes. On the other hand, our experiences [5, 12–14, 16] teach us that for making a uniform homogeneous ion-exchanged glass, this method would not be good enough. The two-sided ion-exchanged glass makes measurements more complicated and confusing, from spectroscopic and photonics points of view.

For making uniform one-sided samples, first, we produced very fine and uniform mixture powder of NaNO_3 and AgNO_3 , with determined weight ratio (Fig. 1). According to our practices from previous works [5, 6, 15, 16], we chose the optimum values for the $\text{NaNO}_3/\text{AgNO}_3$ ratio as 96%/4% (wt%), respectively. Afterward, we put the mixture powder uniformly on the precisely cleaned surface of a soda-lime glass substrate. Subsequently, we put the sample in an electrical oven (our oven has the maximum temperature equal to 1200 °C). After few minutes, the mixture powder melts. As a result of the diffusion, some of the silver ions of the molten mixture salt would exchange with some Na^+ ions of the heated glass substrate. The temperature was chosen as 390 °C, with 2 h duration time. These values are chosen based on our previous researches. The ion-exchange duration time, concentration of AgNO_3 in NaNO_3 mixture, and the temperature of the oven determine the concentration and diffusion depth of the silver ionic atoms and multi-atomic clusters into the glass substrate. At the end of the process, the sample should be cooled very slowly (out of the oven), to prevent any residual mechanical stresses or tensions in the glass, due to thermal shock; otherwise, the sample losses its value as a photonic material and becomes light polarization sensitive.

2.2 He^+ ion-beam production and its interaction with the ion-exchanged glass (ion-beam lithography)

We used an electrostatic accelerator system to produce the He^+ ion beam. This system has three main parts: (1) a penning ion source [26]; (2) a beam extraction; and (3) formation lens system, and finally an acceleration column (Fig. 2). Figure 2 is a schematic drawing of the real accelerator. As it is illustrated, after the entrance of the beam into the target chamber, it passes through an electrostatic scanning system, which scans the beam on the surface of the

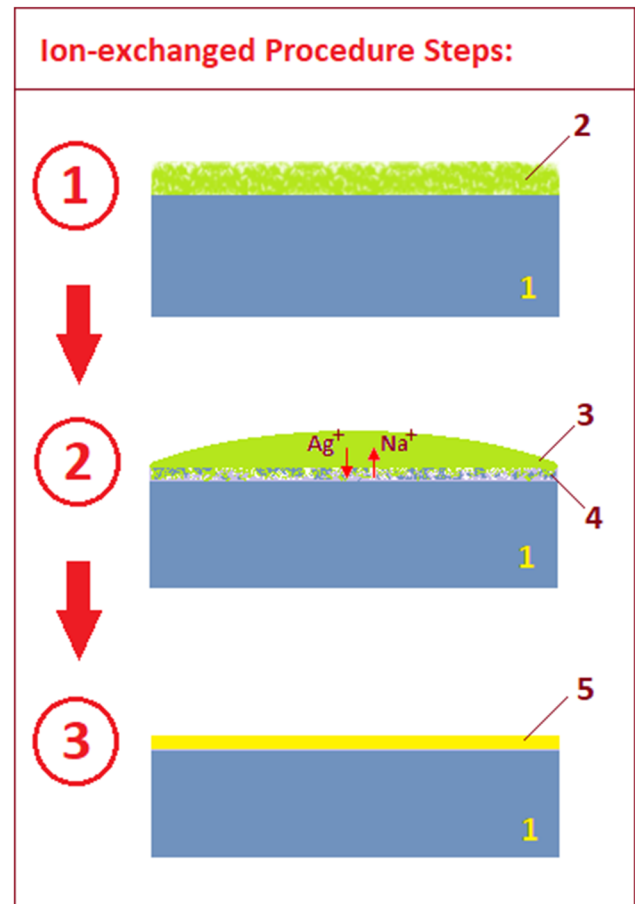


Fig. 1 Ion-exchange procedure steps: 1) covering uniformly, the precisely cleaned surface of soda-lime glass with mixed $\text{NaNO}_3/\text{AgNO}_3$ fine powder; 2) melting the powder and ion exchanging the silver ions with some Na^+ ions of the glass matrix at $T = 390$ °C for 2 h; 3) formation of ion-exchanged layer in vicinity of surface of the sample. At the end of process, the surface of the sample should be washed by a weak acid like diluted HNO_3 : (1) the soda-lime glass matrix; (2) the mixed salt powder; (3) the molten salt; (4) the ion-exchanging layer; and (5) the ion-exchange layer

target in the shape of a square with sides 1 mm long. A hot tungsten filament is placed close to the target for neutralizing the surface of the sample during the bombardment by ions. For the present experiment, the beam current and energy were 10 μA and 40 keV, correspondingly. The scanned area was irradiated by the ion beam with different fluences (number of particles crossing a unit area, usually expressed as the number of particles per cm^2) starting from 2×10^{15} to 1.6×10^{16} (particles/ cm^2) with an increment of 2×10^{15} particles/ cm^2 . For the ion-beam lithography, we obtained best results with 7×10^{15} to 8×10^{15} (particles/ cm^2).

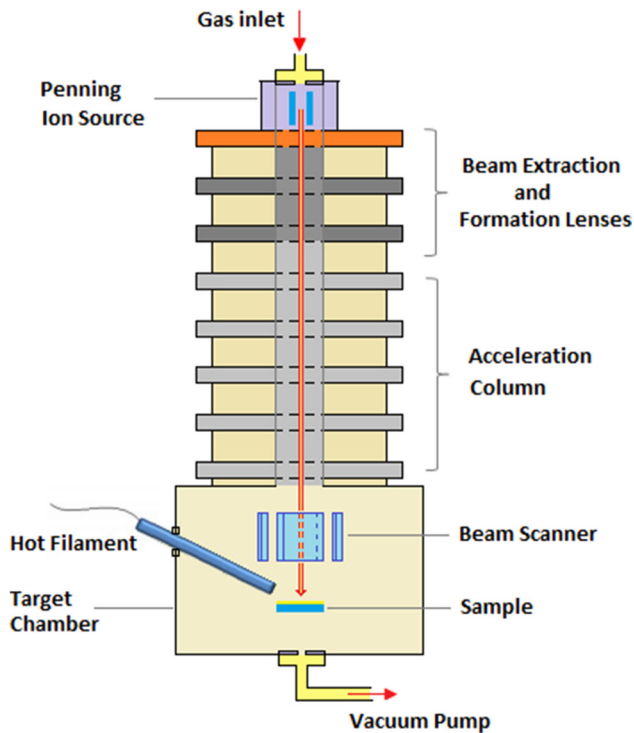
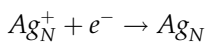


Fig. 2 The generator and accelerator of He^+ beam schema. The actual device has three lenses in beam extraction and formation lens section, and has 10 lenses in the acceleration column

As it is explained in detail in [19], the interaction of the ion beam with the ion-exchanged glass occurs via ionization at first 100 nm depth from the surface of the glass and then through recoil process in depth of about 300–400 nm, where the energy of the ion-beam drops and it comes to stop. Both processes result in generation of electrons which could reduce ionic silver clusters (Ag_N^+) to the neutral ones (Ag_N):



The average size of formed neutral silver clusters due to the interaction is measured and calculated in [19] (using XRD analysis and Scherrer's equation) about $D_{\text{av.}} \simeq 1.00$ nm. This leads to an increase of refractive index up to $n_{\text{max}} = 2.16$ (the initial refractive index of the ion-exchanged glass was $n_I = 1.57$). Such difference in the refractive index ($\Delta n_{\text{max}} = n_{\text{max}} - n_I = 0.585$) is good enough for causing diffraction of a probe light from the boundary of the two area with different refractive indices. The formation of the neutral silver nanoparticles could be confirmed by appearance of a surface plasmon resonance peak [10] in the absorption spectra of the samples after the

interaction with the He^+ beam (Fig. 3). We put a simple metallic mask (a coating of chrome with 250 nm thickness) on half of the ion-exchanged glass to form an edge (Fig. 4). As it can be seen, in addition to the change of the refractive index and absorption, the porosity of the surface of the interacted area with the ion-beam changes, as well (reduced). The corresponding changes in the index of refraction of the samples before and after the interaction are shown in Fig. 5. Refraction Indices are measured by measuring the Brewster's angle for each half, separately. The refractive indices are also measured using reflectance (R) and absorption coefficient described in Ref. [27]. The index of refraction dispersion after the interaction, which is reported in Fig. 5, was confirmed by measurement using the above-mentioned method. It is in good agreement with the similar data reported in Ref. [27]. In this method, the index of refraction (n) can be determined by measuring R and extinction coefficient (k , $k = \frac{\alpha}{4}$, where α is the absorption coefficient [28]). They are related to each other as follows [27, 29]:

$$n = \frac{(1 + R) + \sqrt{4R - (1 - R)^2 k^2}}{(1 - R)} \quad (1)$$

Results of relation (1) confirm the results obtained by Brewster's angle measurement (Fig. 5). We did not

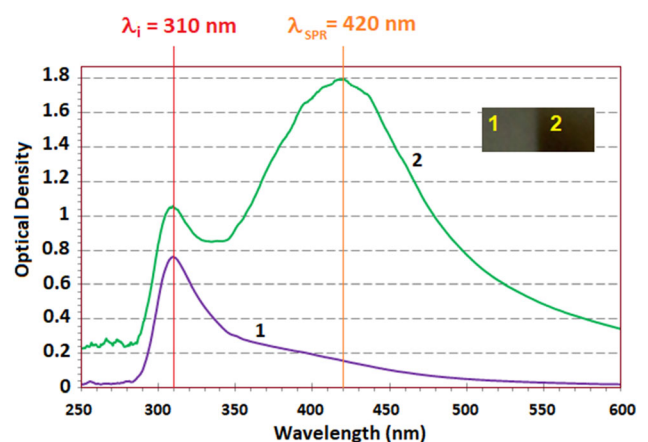


Fig. 3 Absorption spectra of the ion-exchanged glass: (1) before the interaction with He^+ beam, (2) after the interaction. The inset: corresponding areas on the sample (1 and 2) are shown, accordingly. After the interaction, appearance of characteristic surface plasmon resonance peak for neutral silver nanoparticles in wavelength $\lambda_{\text{SPR}} = 420$ nm is observed

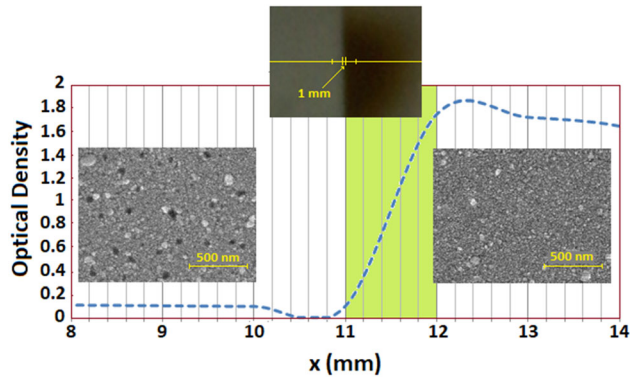


Fig. 4 SEM images of non-interacted (left SEM image) and interacted (right SEM image) areas on the surface of the sample, half of which was covered by a metallic layer of Chrome. Corresponding absorptions (the curve shown by “- -”) are measured for two sides at wavelength $\lambda_{SPR} = 420$ nm. It can be seen porosity of interacted area is less than that of non-interacted side of the sample

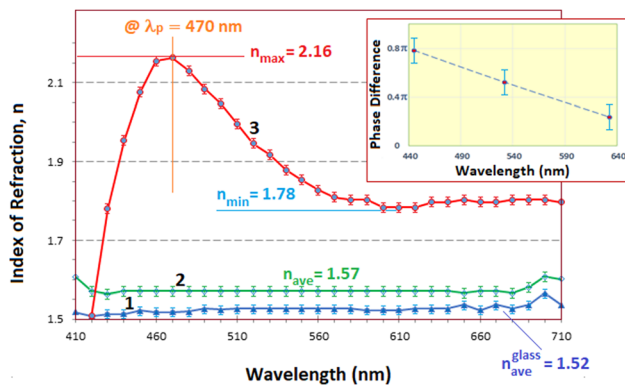


Fig. 5 Dispersion of induced index of refraction change due to the interaction with He⁺ beam: (1) index of refraction of the used soda-lime glass for visible region of spectrum; (2) index of refraction for the same glass matrix after the ion-exchange process. Both do not exhibit remarkable dispersion; (3) index of refraction after interaction with the ion beam. In wavelengths close to the surface plasmon resonance peak the change in index of refraction is maximum. The inset shows phase difference between interacted and non-interacted parts of the samples, at three different probe light wavelengths: $\lambda_B = 445$ nm, $\lambda_G = 532$ nm, and $\lambda_R = 632.8$ nm

use the Wemple-DiDomenico model, because it is more precise for semiconductor materials rather than amorphous materials (like glass). Its results also do not match with our experimental data, especially in short wavelengths of the spectrum.

Hence, if one could pattern the index of refraction in this medium, it would be possible to fabricate optical diffractive phase elements, which is the

purpose of the present work. On the other hand, the dispersion of the refractive index after the interaction (Fig. 5) affects the range of functionality of the fabricated diffractive elements from spectroscopy point of view.

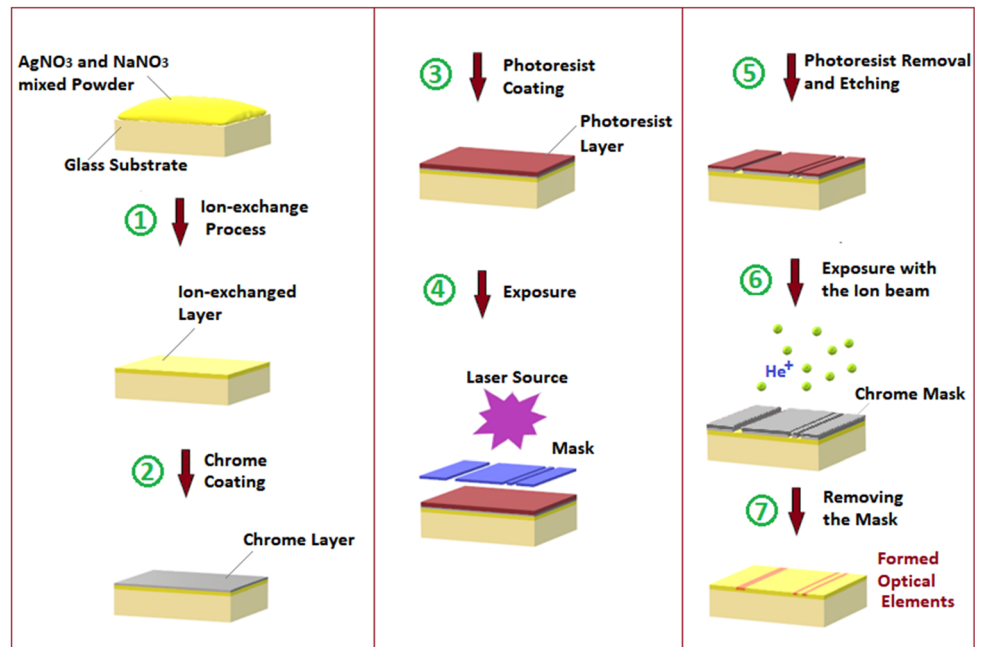
2.3 The ion-beam lithography in ion-exchanged glass process

As a general definition, conventional optical lithography is a process used to pattern some parts on a thin film, a surface, or the bulk of a substrate. In this method, one uses light to transfer a geometric pattern from a photomask to a light-sensitive material, which is called photoresist. Then, a series of chemical treatments would be conducted. The treatment results in etching the exposure pattern into the material or allows deposition of a new material in the desired pattern upon the material set under the photoresist layer [30].

In our developed ion-beam lithography method, first, we use optical lithography to put a metallic mask on the ion-exchanged glass substrate. Then we expose the sample by the He⁺ beam produced by the accelerator, which we explained in section (b). The details of the ion-beam lithography process are shown in Fig. 6. In fact, in our experiments, the silver-ion-exchanged glass plays the role of the photo-sensitive material, where the final pattern should be formed.

In first step, we ion-exchange the glass substrate as was explained in section (a). Next, we coat the produced ion-exchanged glass with a chrome thin film (thickness ~ 250 nm) by sputtering method ($p_{vacuum} \sim 10^{-5}$ mmHg). In third step, we cover the chrome layer with photoresist (in our case: S1813) by spin coating. Warming the photoresist layer up to 115 °C for 20 min helps us to obtain a more uniform photoresist layer. Next, we create a mask’s image on the surface of the sample as small as possible. The light source used for the optical lithography was a violet diode laser with the wavelength of $\lambda_V = 405$ nm and power of $P_V = 100$ mW. The exposure time was 3 min. In this way, the intended pattern (slit, double slit, grating, zone plate, etc.) transfers on the photoresist layer (step 4 in Fig. 6). Now, we should first remove the exposure parts of the photoresist and then remove the parts of the chrome layer, which were under exposure parts of the photoresist (step 5

Fig. 6 Steps of ion-beam lithography: (1) ion-exchange process; (2) chrome coating on the ion-exchanged glass; (3) photoresist coating on the Chrome layer; (4) exposure by violet light ($\lambda_V = 405$ nm and $P_V = 100$ mW) to create the image of the optical element mask on the photoresist layer; (5) photoresist removal and etching the naked chrome layer; (6) exposure by the He^+ beam; and (7) removal the metallic mask



of Fig. 6). To remove the photoresist, we used diluted NAOH solution (0.1 mol/L), and for etching the chrome parts, we used Ceric ammonium nitrate ($(\text{NH}_4)_2\text{Ce}(\text{NO}_3)_6$) mixed with dilute acid nitric. Thus, in this step, we have a miniaturized metallic negative pattern (the mask) on the ion-exchanged glass (step 5 of Fig. 6). Before bombardment by the ion beam, we should remove the unexposed part of the photoresist with acetone. Some of the printed photomasks on plastic transparent sheets for step 4 are shown in Fig. 7. Now, the masked ion-exchanged glass samples are bombarded with the He^+ ion beam (step 6 of Fig. 6) for the ion-beam lithography. As a result, the unmasked parts of the sample interact with the ion beam and their absorption and refractive indices change as we explained earlier (Figs. 3, 4 and 5). After the bombardment, we remove the chrome mask with the same etching solution (Ceric ammonium nitrate + HNO_3 + H_2O).

There are two important points, which should be considered during the *ion-beam lithography* to obtain good and sharp edges of the transferred patterns that make them diffractive elements with good quality: (1) quality of the metallic mask's edges; (2) the amount of divergence or convergence of the ion beam. If the chemical processes of photoresist removal and etching is carried on with low accuracy, or one does not pay attention to the exact percentage of solvents and

etchants and the temperature of the processes, the edges of the metallic masks may be obtained oblique (Fig. 8-2-a), repelled, or rough. We call it an imperfect edge. Such edges cause a shadow in the vicinity of the mask's edges which lowers the quality of the final produced optical diffractive elements and reduces their diffraction efficiency. Convergence or divergence of the ion beam also causes imperfection at the edges (Figs. 8-3). Thus, controlling the ion-beam quality is one of the important parameters for obtaining the best results. The uniformity, quality, and thickness of the metallic masks are also very important parameters in the ion-beam lithography method.

2.4 Diffraction patterns from the produced optical phase elements

As a first example of the produced diffractive optical elements, we studied the Fraunhofer diffraction, with the setup shown in Fig. 9a from five slits (each slit has 100 μm width and 500 μm distance from the neighboring one) (Fig. 9b) and a diffraction grating with 10 lines/mm (Fig. 9c, d). As it can be seen, the expected diffraction patterns are observed. A standard setup for observing the Fraunhofer diffraction patterns is applied (Fig. 9a), and as a screen, a

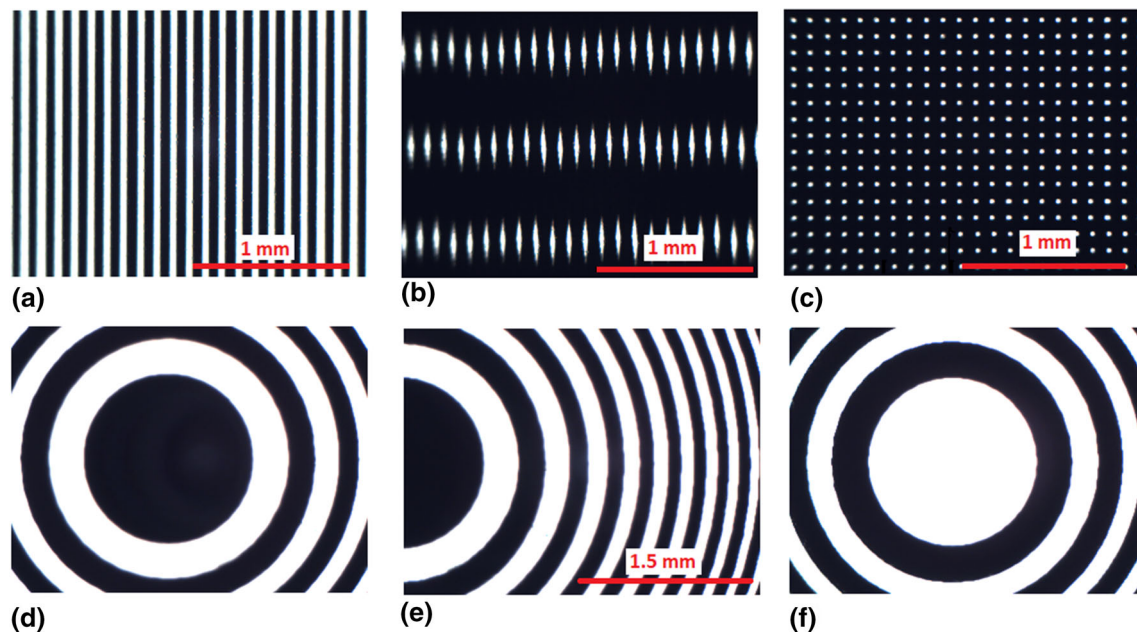


Fig. 7 The printed photomasks on plastic transparent sheets for step 4 of Fig. 6: **a** 10 lines/mm grating; **b** two crossed linear gratings (with 10 lines/mm and angle $\theta = 10^\circ$ between them);

c square grid with $25 \mu\text{m}$ size of dots and $100 \mu\text{m}$ distance between neighboring dots; **e** and **f** zone plate with closed central zone (CZP); **g** zone plate with open central zone (OZP)

lensless DSLR camera is used. Figure 9d shows the same diffraction pattern of Fig. 9c, which is the diffraction pattern from the fabricated diffraction grating with 10 lines/mm, but with lower intensity of the source (a standard sodium lamp with an adjustable slit in front of it for intensity control).

In Fig. 10, diffraction pattern of the same five slits with its intensity distribution (Fig. 10b) is shown. The middle-right inset in Fig. 10 shows the microscopic image of the fabricated five slits.

In Fig. 11, diffraction patterns from the fabricated grating for a He–Ne Laser beam ($\lambda_{\text{red}} = 632.8 \text{ nm}$, Fig. 11a) and an Nd⁺-YAG laser beam ($\lambda_{\text{green}} = 532 \text{ nm}$, Fig. 11b) are shown. In Fig. 11c, the microscopic image of the produced grating is shown. The dark parts in Fig. 11c are the interacted parts of the ion-exchanged glass with the He⁺ ion beam. The same setup of Fig. 11 was used to observe the diffraction patterns from single slits with different widths (Fig. 12a'–c'). The microscopic images of the corresponding slits are shown in Fig. 12a–c with widths $200 \mu\text{m}$, $100 \mu\text{m}$, and $50 \mu\text{m}$, respectively. The scale of the microscope (Fig. 12d) is shown for comparison.

Another diffractive element produced by the ion-beam lithography in ion-exchanged glass was a square grid made of points with diameter of $25 \mu\text{m}$ with grid constant of $100 \mu\text{m}$ (Fig. 13a). Corresponding diffraction patterns are shown in Fig. 13b and c for a He–Ne laser beam and Fig. 13d for a Nd⁺-YAG laser beam, accordingly. In Fig. 13c, the undiffracted beam is eliminated to observe only the diffracted light. As it can be seen, the phase grid has diffracted the incident probe light effectively. In Fig. 13e, diffraction of a He–Ne laser beam from the five slits, described earlier (Fig. 10), can be seen. Figure 13f shows diffraction from the pattern made by crossing two gratings with angle $\theta = 10^\circ$ between them. Insets of Fig. 13e and f show microscopic images of their corresponding fabricated diffractive elements.

The last fabricated phase diffractive element, which is one of the important optical elements, was the Fresnel zone plate (Fig. 14). Two types of zone plates were made: (1) a zone plate with closed central zone (Figs. 14-1a), we named CZP and a zone plate with open central zone (Figs. 14-1b) which we named

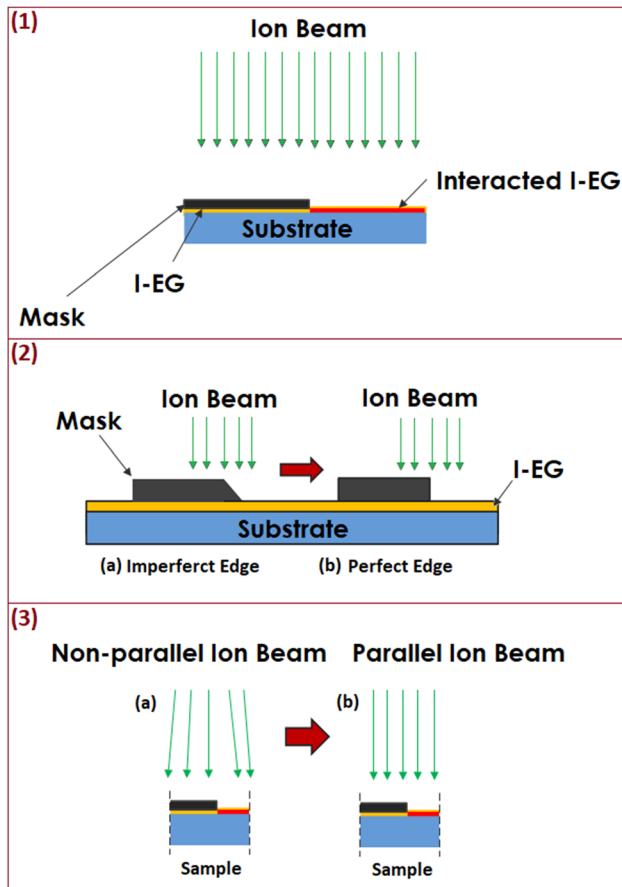


Fig. 8 (1) The area of the ion-exchanged layer (I-EG) under the metallic mask does not interact with the ion beam; (2) Imperfect edges of the metallic mask; or (3) unparallel ion beam, reduces the quality of the element fabricated by *Ion-beam lithography*

OZP. Figures 14-2 is diffraction pattern from CZP (Fig. 14-1a) at its first focal point ($z = 42$ cm), and Fig. 14-3 is the diffraction pattern from the OZP at its first focal point. Figure 14-4a' and b' shows the diffraction patterns of Figs. 14-1a and 1b accordingly, in distances less than the first focal distances for CZP and OZP. Focusing the probe beam by the zone plates is observed (Fig. 14). Ion-beam lithography quality is restricted by the optical lithography limitation for the metallic mask preparation procedure. The degree of purity and quality of used materials for etching and removal processes also play essential roles for obtaining good results of ion-beam lithography.

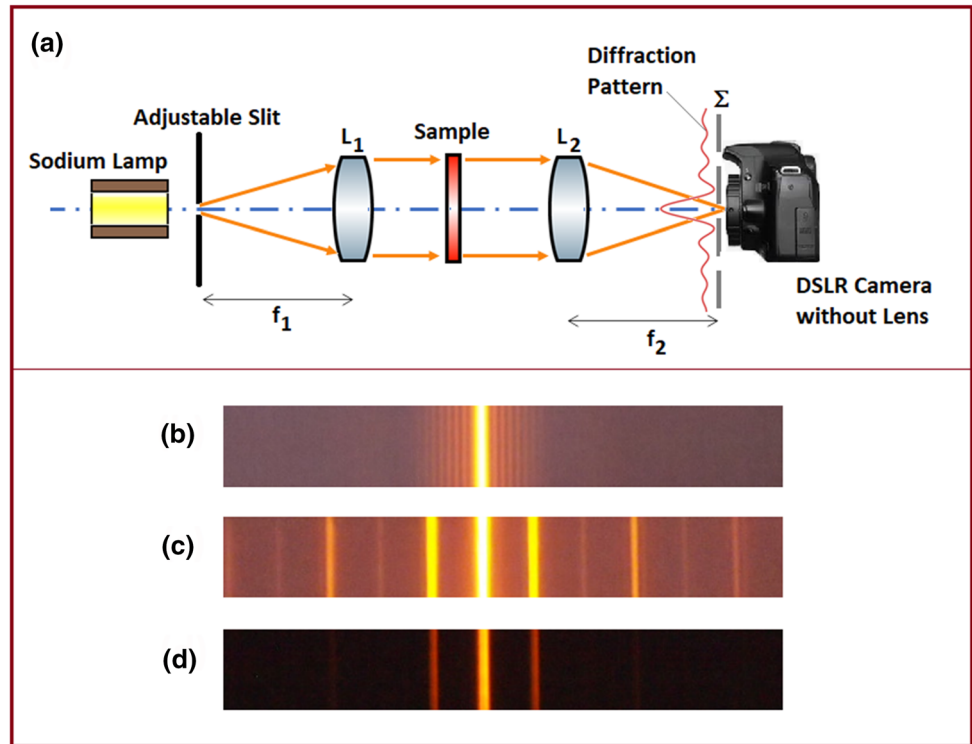
3 Discussion

An increase in the index of refraction, after the formation of neutral silver nanoclusters embedded in a dielectric matrix, has been observed in our previous researches [5, 6, 14, 16, 19]. It has been also discussed by other researchers [31–33] that the formation of metallic nanoparticles in a dielectric matrix increases the average dielectric constant (relative permittivity, ϵ_r), which in its turn, increases the index of refraction of the medium, $n = \sqrt{\epsilon_r}$ [34]. Apart from the variation of n , we observed an increase in absorption spectra of the interacted areas of the samples, which is related to surface plasmon resonance of the formed silver nanoparticles (Fig. 3). In other words, the produced diffractive phase elements using ion-beam lithography influence the intensity distribution and variation of the phase of the probe light, which both enhance the diffraction efficiency of the fabricated optical elements.

Diffraction efficiency, $\eta (= \frac{I_1}{I_0})$, where I_0 is the intensity of the incident probe light and I_1 is the intensity of the first order of the diffraction from the grating), of the fabricated grating (10 lines/mm) for three different probe lights are measured and reported in Table 1. It is clear that increasing the number of lines per length improves the diffraction efficiency of a grating. Hence, the fabrication of grating with a higher number of lines/mm is under investigation by our group. The quality of the produced grating can be increased by improvement of lithography techniques, especially the metallic mask production and its removal procedure. Using another metal for the mask could be one of the answers. This point is also under investigation.

As it can be concluded from Fig. 5, Table 1, the wavelength (i.e., $\lambda_B = 445$ nm) close to the wavelength for which the induced change in the index of refraction is maximum (i.e., $\Delta n_{\max} = 0.59 @ \lambda_p = 470$ nm) diffraction efficiency is the highest ($\eta_B \sim 19.5\%$) and for the wavelength $\lambda_R = 632.8$ nm, for which the induced change in the index of refraction is minimum ($\Delta n_{\min} = 0.15$), the η is the lowest ($\eta_R \sim 3\%$). That is, larger induced refractive index difference leads to higher diffraction efficiency for the phase grating which is fabricated by our *ion-beam lithography* method. The reason for that could be explained as follows: For fabricated phase diffractive elements, high phase difference, $\Delta\phi$, (phase difference between

Fig. 9 a Setup for observing Fraunhofer diffraction from the fabricated elements. L_1 and L_2 are lenses and f_1 and f_2 , both equal to 10 cm, are their focal distances, accordingly; **b** diffraction pattern from five slits; **c** diffraction pattern from fabricated 10 lines/mm diffraction grating; **d** the diffraction pattern from the same grating of (c) but with lower intensity of the sodium lamp, which obtained by adjustable slit shown in (a)



light beams passing through the two sides of border of interacted and non-interacted areas on the samples) leads to the higher diffraction efficiency [35]. For phase difference, we have

$$\Delta\phi = \frac{2\pi}{\lambda}(n_2 - n_1)d, \tag{2}$$

where n_2 is the refractive index of interacted area, n_1 is the refractive index of non-interacted area, d is the geometrical path length, which in our case is the thickness of the interacted area, i.e., $d \sim 500$ nm) and λ is the wavelength of the probe light.

On the other hand, we know that the phase of the probe light after passing through the sample is equal to $\delta = k \cdot \Delta$, where $k = \frac{2\pi}{\lambda}$ is the wave number and $\Delta = n \cdot d$ is the optical path (n is the index of refraction of medium) [36]. The relative index of refraction, $n_{21} = \frac{n_2}{n_1}$, which is the ratio of refractive indices could be taken as determining factor for diffraction efficiency. If we use the relative index of refraction, n_{ij} , to find the relative optical path Δ_{ij} of the interacted area, then we could determine the phase δ for the probe beam after passing through that part of the samples. We found that for shorter wavelengths close to the wavelength corresponding to the maximum of the induced index of refraction, we would have larger phase difference $\Delta\phi$, which provides higher

diffraction efficiency. The summary of the above discussion is presented in Table 1. The inset of Fig. 5 shows the variation of the phase difference between two interacted and non-interacted parts with the wavelength of the probe beam. This result is well consistent with the dispersion of the induced refractive indices after the interaction. The reported induced n in the present article has tolerance less than 0.5% from the n reported in our previous related work [19].

Any imperfection in edges of the lithography patterns reduces diffraction efficiency of the produced elements, dramatically. Imperfect edges diffract the incident light to directions that are not useful and increase the loss, leading to reduction of η . Therefore, this method requires lots of care and accuracy in each step of the process.

Using high-quality optics and better techniques for printing a high-quality photomask, and also the quality of the ion beam, accuracy in metallic mask coating, and stable thermal conditions with controlled chemical reactions during removal/etching the materials are the most important parameters for fabrication of functional optical diffractive elements.

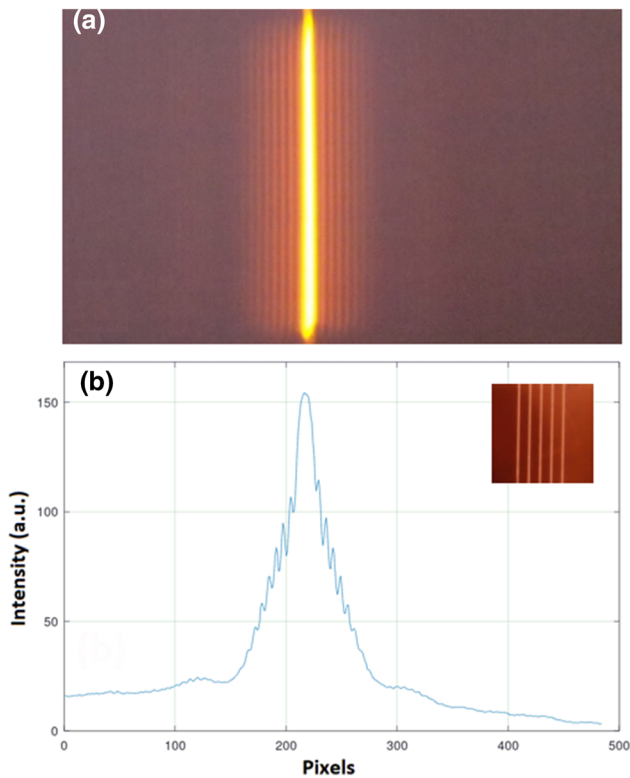


Fig. 10 **a** Fraunhofer diffraction from five slits, using the setup shown in Fig. 9; **b** the intensity distribution of the diffraction pattern of (a). The middle-right inset shows the microscopic image of the five slits, each slit has 100 μm width, and distance with neighboring slit is 500 μm

4 Conclusions

As a summary, results of interaction of a low-energy He^+ beam ($E \sim 40 \text{ keV}$), with silver-ion-exchanged glass were used to establish an *ion-beam lithography* method to fabricate miniaturized optical diffractive phase elements, such as slits, gratings, grids, and Fresnel zone plates. The interaction results in reduction of ionic Ag_N^+ nanoparticles to the neutral ones, Ag_N , which in turn increases the index of refraction of the interacted area on the samples [19]. The absorption of interacted area also increases and shows a characteristic surface plasmon resonance peak (Fig. 3), which is an indication of the formation of neutral silver nanoparticles as a result of the interaction [10]. On the other hand, a metallic mask could stop the ion beam [19], which helps us to fabricate optical phase diffractive elements by ion-beam lithography. The diffraction patterns from the produced elements show good quality (Figs. 9, 10, 11, 12, 13 and 14), encouraging us to further develop the technique.

A remarkable dispersion was observed for the induced refractive indices changes. The change in the induced refractive index is maximum for wavelengths close to the surface plasmon peak of Ag nanoparticles (embedded in a glass matrix). As a

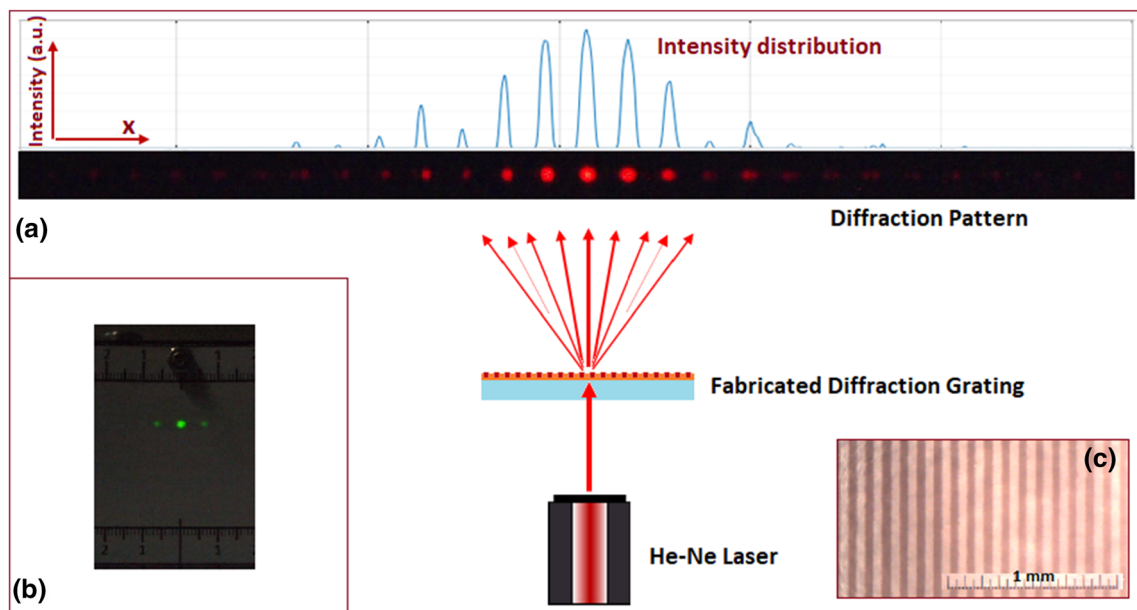


Fig. 11 Diffraction patterns of **a** He–Ne laser beam ($\lambda_{\text{red}} = 632.8 \text{ nm}$) and **b** diode pump Nd^+ -YAG laser beam ($\lambda_{\text{green}} = 532 \text{ nm}$) from the produced grating with 10 lines/mm. Intensity distribution

of the diffraction pattern of (a) is shown at the top of the image (a). The corresponding microscopic image of the grating is shown in (c)

Fig. 12 Diffraction patterns (a'–c') from slits with widths 200 μm , 100 μm , and 50 μm , accordingly. Relevant microscopic images are shown in (a–c). The scale of the microscope is shown in (d) for comparison

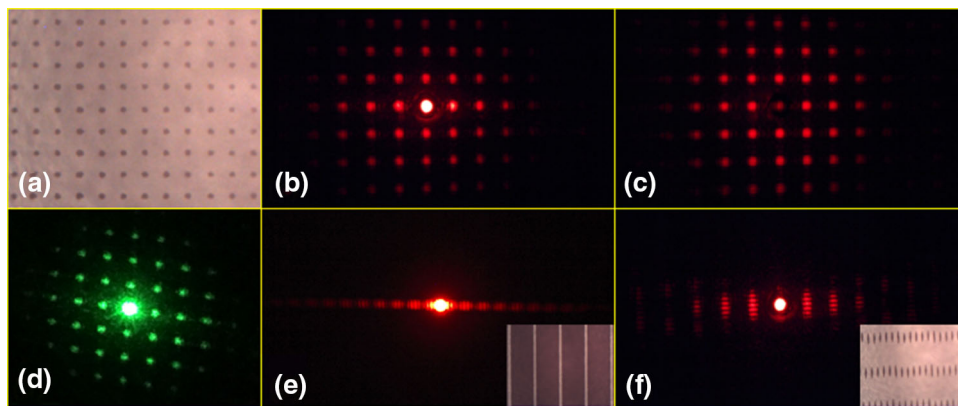
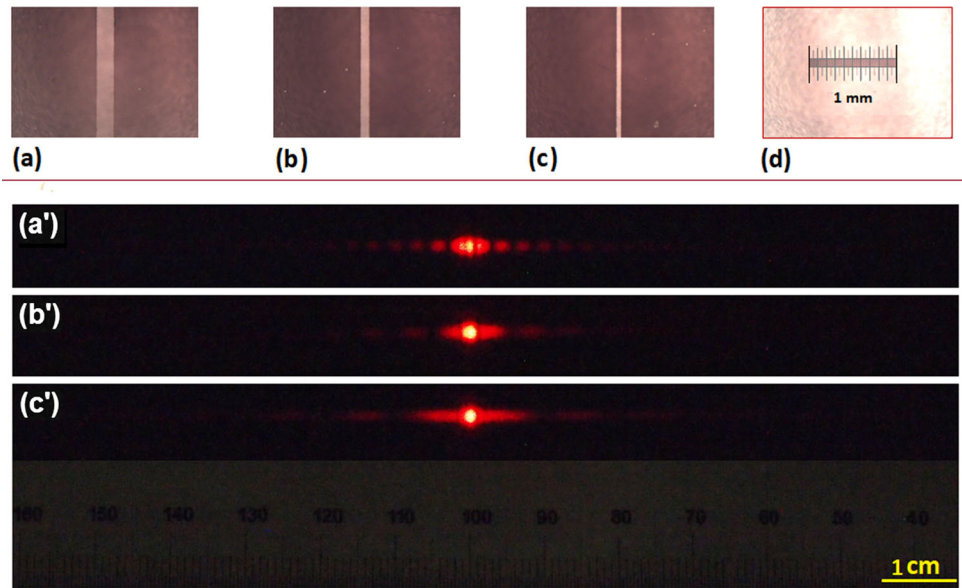


Fig. 13 **a** The microscopic image of fabricated square grid by ion-beam lithography. Each point of grid has 25 μm size with 100 μm distance between them; **b** corresponding diffraction pattern of He–Ne laser beam from the grid; **c** is the same pattern of (b), with faded undiffracted beam on the screen; **d** diffraction from the same grid for Nd^+ -YAG laser beam; **e** diffraction of He–Ne laser beam

from five slits with 50 μm width for each slit and 500 μm distance between them; **f** diffraction pattern from two cross gratings with 10 lines/mm with angle $\theta = 10^\circ$ between them. The corresponding microscopic images of produced elements are shown as insets in (e) and (d) images

consistent result, the diffraction efficiency of the fabricated diffraction gratings is also the largest at these wavelengths. A remarkable quality of the produced elements could be achieved, by using better optics for lithography of the mask and high-quality and pure chemical materials for etching and removal procedures. The controlled temperature during the etching process is also an important parameter.

The fabricated phase diffractive elements are waterproof, scratch resistant, and chemically

stable with acceptable diffraction efficiencies, which are important advantages of *ion-beam lithography in ion-exchanged glasses*, from the application point of view. The introduced method could be considered as an effective way to produce meta-materials, functioning in the visible region of the spectrum, which is under investigation by our group.

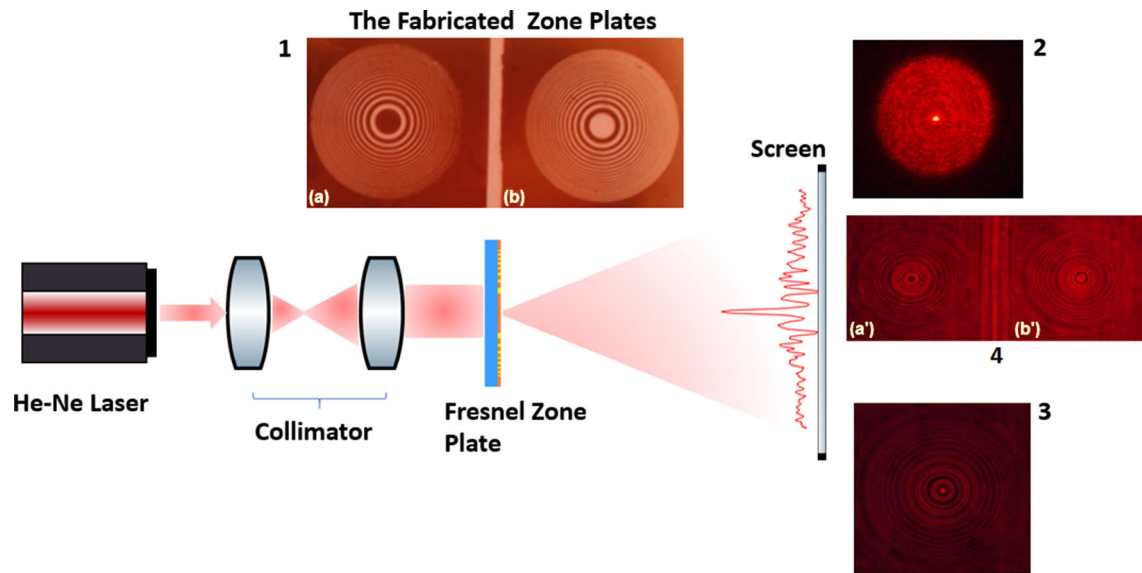


Fig. 14 Setup for observing the diffraction from the fabricated zone plates: (1) microscopic images of fabricated zone plates with **a** closed central zone (CZP) and **b** open central zone (OZP); (2) diffraction pattern at first focus point for CZP; (3) diffraction

pattern at first focus point for OZP; (4a') and (4b') are diffraction patterns before the focus point for CZP and OZP, accordingly. The measured intensity distribution of (3) is drawn on the screen of the setup scheme

Table 1 Diffraction efficiencies of the produced gratings (h) for three different light sources

The light source	Probe light Wavelength (nm)	Induced refractive index difference, Δn	Relative refractive index $n_{ij} = n_i / n_j$	$\Delta_{ij} = n_{ij} \cdot d$ (nm) @ $d \sim 500$ nm	Phase after the interacted part, δ	$\Delta\phi$	Diffraction efficiency, η (%)
Diode Laser	445	0.59 ± 0.02	1.223	611.5	2.74π	0.786π	19.5 ± 1.5
Diode pumped Nd ⁺ -YAG	532	0.28 ± 0.02	1.178	589.0	2.21π	0.524π	12.2 ± 0.5
He-Ne laser	632.8	0.15 ± 0.02	1.095	547.5	1.72π	0.238π	3.0 ± 0.3

Dn is Induced refractive index difference, n_{ij} relative refractive index of the exposed part relative to the unexposed part of the samples, D_{ij} is the optical path difference corresponding to n_{ij} , d is according phase after the optical path D_{ij} , and Df is the phase difference between the light which is passed through the exposed part relative to the light which is passed through the unexposed part

Acknowledgements

Authors would like to thank Dr. Khosrow Hassani for his valuable discussions and advices, and also Dr. Abbas Saberi for his financial support of XRF measurements, both of them from Department of Physics of University of Tehran, Iran.

Data availability

The data that support the findings of this study are available from the corresponding author upon reasonable request.

Declarations

Conflict of interest The authors have no conflict of interest to declare that are relevant to the content of this article.

References

1. S.R. Friberg, P.W. Smith, Nonlinear optical glasses for ultrafast optical switches. *IEEE J. Quantum Electron.* **QE-23**, 2089–2092 (1987)
2. F. Caccavale, G. De Marchi, F. Gonella, P. Mazzoldi, C. Meneghini, A. Quaranta, G.W. Arnold, G. Battaglin, G.

- Mattei, Irradiation-induced Ag-colloid formation in ion-exchanged soda-lime glass. *Nucl. Instrum. Meth. Phys. Res.* **96**, 382–386 (1995)
3. F. Gonella, G. Mattei, P. Mazzoldi, E. Cattaruzza, G.W. Arnold, G. Battaglin, P. Calvelli, R. Polloni, B. Bertonecello, R.F. Haglund Jr., Interaction of high-power laser light with silver nanocluster composite glasses. *Appl. Phys. Lett.* **69**, 3101–3103 (1996)
 4. 5. A.L. Stepanov, V.N. Popok, D.E. Hole, A.A. Bukharaev, Interaction of high-power laser pulses with glasses containing implanted metallic nanoparticles. *Phys. Solid State* **43**, 2192–2198 (2001)
 5. A. Nahal, H.R.M. Kkhalesifard, J. Mostafavi-Amjad, Photothermal-induced dichroism and micro-cluster formation in Ag⁺-doped glasses. *Appl. Phys. B* **79**, 513–518 (2004)
 6. A. Nahal, J. Mostafavi-Amjad, A. Ghods, M.R.H. Khajehpour, S.N.S. Reihani, M.R. Kolahchi, Laser-induced dendritic microstructures on the surface of Ag⁺-doped glass. *J. Appl. Phys.* **100**, 053503 (2006)
 7. A. Pinchuk, A. Hilger, G. von Plessen, U. Kreibig, Substrate effect on the optical response of silver nanoparticles. *Nanotechnology* **15**, 1890–1896 (2004)
 8. M.C. Gupta, J. Ballato, *The Handbook of Photonics* (CRC Press, Taylor & Francis Group, Boca Raton, 2007)
 9. S.I. Najaf, *Introduction to Glass Integrated Optics* (Artech House, Norwood, 1992)
 10. U. Kreibig, M. Vollmer, *Optical Properties of Metal Clusters* (Springer, Berlin, Heidelberg, New York, 1995)
 11. P.L. Inácio, B.J. Barreto, F. Horowitz, R.R.B. Correia, M.B. Pereira, Silver migration at the surface of ion-exchange waveguides: a plasmonic template. *Opt. Mater. Express* **3**, 390–399 (2013)
 12. A. Nahal, A. Jalehdost, Kh Hassani, A. Farokhniaee, Variation of index of refraction in the ion-exchanged glasses with the evolution of ionic and neutral silver nano-clusters. *Eur. Phys. J. Appl. Phys.* **53**, 10701 (2011)
 13. A. Nahal, K. Shapoori, Linear dichroism, produced by thermoelectric alignment of silver nanoparticles on the surface of ion-exchanged glass. *Appl. Surf. Sci.* **255**, 7946–7950 (2009)
 14. A. Nahal, R. Talebi, M.F. Miri, Thermo-electric-induced dichroism in ion-exchanged glasses: a candidate mechanism for the alignment of silver nanoparticles. *Appl. Phys. A* **106**, 941–947 (2012)
 15. A. Nahal, H.R.M. Kkhalesifard, Beam power-dependent laser induced fluorescence radiation quenching of silver-ion-exchanged glasses. *Opt. Mater.* **29**, 987–994 (2007)
 16. A. Nahal, F. Moslehirad, Laser-induced anisotropy in Ag⁺-doped glasses. *J. Mater. Sci.* **42**(12), 9075–9082 (2007)
 17. G. Sathiyapriya, K.A. Naseer, K. Marimuthu, E. Kavaz, A. Alalawi, M.S. Al-Buriahi, Structural, optical and nuclear radiation shielding properties of strontium barium borate glasses doped with dysprosium and niobium. *J. Mater. Sci. Mater. Electron.* **32**, 8570–8592 (2021)
 18. K.S. Shaaban, Y.B. Saddeek, Effect of MoO₃ content on structural, thermal, mechanical and optical properties of (B₂O₃–SiO₂– Bi₂O₃–Na₂O–Fe₂O₃) glass system. *Silicon* **9**(5), 785–793 (2017)
 19. A. Nahal, M. Mahjour-Shafei, S.R. Hosseini, Index of refraction variation and photoluminescence quenching in silver ion exchanged glasses, due to interaction with low energy He⁺ beam. *J. Mater. Sci.: Mater. Electron.* **31**, 5499–5510 (2020)
 20. A. Nahal, F. Moslehirad, Laser-induced anisotropy in Ag⁺-doped glasses. *J. Mater. Sci.* **42**(12), 9075–9082 (2007)
 21. I. Antonov, F. Bass, Y. Kaganovskii, M. Rosenbluh, Fabrication of microlenses in Ag-doped glasses by a focused continuous wave laser beam. *J. Appl. Phys.* **93**, 2343 (2003)
 22. M. Heinz, J. Meinertz, M. Dubiel, J. Ihlemann, Excimer laser induced spatially resolved formation and implantation of plasmonic particles in glass. *Nanomaterials* **8**, 1035 (2018)
 23. L.A.H. Fleming, S. Wackerow, A.C. Hourd, W.A. Gillespie, G. Seifert, A. Abdolvand, Diffractive optical element embedded in silver doped nanocomposite glass. *Opt. Express* **20**, 22580 (2012)
 24. H. Hofmeister, S. Thiel, M. Dubiel, E. Schurig, Synthesis of nanosized silver particles in ion-exchanged glass by electron beam irradiation. *Appl. Phys. Lett.* **70**, 1694 (1997)
 25. R. Kumar, M. Chauhan, M.G. Moinuddin, S.K. Sharma, K.E. Gonsalves, Development of nickel-based negative tone metal oxide cluster resists for sub-10 nm electron beam and helium ion beam lithography. *ACS Appl. Mater. Interfaces* **12**, 19616–19624 (2020)
 26. M. Mahjour-Shafei, H. Noori, A.H. Ranjbar, Influence of magnetic field on the electric breakdown in penning ion source. *Rev. Sci. Instrum.* **82**, 113502 (2011)
 27. A.S. Sonal, S. Aggarwal, Optical investigation of soda lime glass with buried silver nanoparticles synthesized by ion implantation. *J. Non-Crystal. Sol.* **485**, 57–65 (2018)
 28. J. Garcia Sole, L.E. Bausa, D. Jaque, *An Introduction to the Optical Spectroscopy of Inorganic Solids* (Wiley, England, 2005)
 29. M. Fox, *Optical Properties of Solids* (Oxford University Press, Oxford, 2001)
 30. R.C. Jaeger “Lithography”. *Introduction to Microelectronic Fabrication* (2nd edn.) (Upper Saddle River: Prentice Hall, 2002)
 31. J.C.M. Garnett, Colours in metal glasses and in metallic films. *Philos. Trans. R. Soc. Lond.* **203**, 385–420 (1904)
 32. D.A.G. Bruggeman, Berechnung verschiedener physikalischer Konstanten von heterogenen Substanzen.

- I. Dielektrizitätskonstanten und Leitfähigkeiten der Mischkörper aus isotropen Substanzen. *Ann. Phys. Leipzig* **24**, 636–664 (1935). (in German)
33. G.A. Niklasson, C.G. Granqvist, O. Hunderi, Effective medium models for the optical properties of inhomogeneous materials. *Appl. Opt.* **20**(1), 26–30 (1981)
34. B.E.A. Saleh, M.C. Teich, *Fundamentals of Photonics*, 3rd edn. (Wiley, Hoboken, 2019)
35. A.Y. Meshalkin, V.V. Podlipnov, A.V. Ustinov, E.A. Achimova, Analysis of diffraction efficiency of phase gratings in dependence of duty cycle and depth. *J. Phys.: Conf. Ser.* **1368**(2), 022047 (2019)
36. F. Pedrotti, L. Pedrotti, L. Pedrotti, *Introduction to Optics*, 3rd edn. (Cambridge University Press, Cambridge, 2017)

Publisher's Note Springer Nature remains neutral with regard to jurisdictional claims in published maps and institutional affiliations.